

Contents lists available at ScienceDirect

# Petroleum Science

journal homepage: www.keaipublishing.com/en/journals/petroleum-science



# Original Paper

# Multi-objective optimization workflow for CO<sub>2</sub> water-alternating-gas injection assisted by single-objective pre-search



Ren-Feng Yang <sup>a</sup>, Wei Zhang <sup>b, c, \*</sup>, Shuai-Chen Liu <sup>b</sup>, Bin Yuan <sup>b, c, \*\*</sup>, Wen-Dong Wang <sup>b</sup>

- <sup>a</sup> CNOOC Research Institute Co., Ltd., Beijing, 100028, China
- <sup>b</sup> School of Petroelum Engineering, China University of Petroleum (East China), Qingdao, 266580, Shandong, China
- <sup>c</sup> State Key Laboratory of Deep Oil and Gas, China University of Petroleum (East China), Qingdao, 266580, Shandong, China

#### ARTICLE INFO

# Article history: Received 2 January 2025 Received in revised form 25 March 2025 Accepted 26 March 2025 Available online 26 March 2025

Edited by Yan-Hua Sun

Keywords: CO<sub>2</sub>-WAG CO<sub>2</sub> storage Multi-objective optimization Convergence criterion

#### ABSTRACT

CO<sub>2</sub> Water-Alternating-Gas (CO<sub>2</sub>-WAG) injection is not only a method to enhance oil recovery but also a feasible way to achieve CO<sub>2</sub> sequestration. However, inappropriate injection strategies would prevent the attainment of maximum oil recovery and cumulative CO<sub>2</sub> storage. Furthermore, the optimization of CO<sub>2</sub>-WAG is computationally expensive as it needs to frequently call the compositional simulation model that involves various CO<sub>2</sub> storage mechanisms. Therefore, the surrogate-assisted evolutionary optimization is necessary, which replaces the compositional simulator with surrogate models. In this paper, a surrogate-based multi-objective optimization algorithm assisted by the single-objective pre-search method is proposed. The results of single-objective optimization will be used to initialize the solutions of multi-objective optimization, which accelerates the exploration of the entire Pareto front. In addition, a convergence criterion is also proposed for the single-objective optimization during pre-search, and the gradient of surrogate models is adopted as the convergence criterion. Finally, the method proposed in this work is applied to two benchmark reservoir models to prove its efficiency and correctness. The results show that the proposed algorithm achieves a better performance than the conventional ones for the multi-objective optimization of CO<sub>2</sub>-WAG.

© 2025 The Authors. Publishing services by Elsevier B.V. on behalf of KeAi Communications Co. Ltd. This is an open access article under the CC BY-NC-ND license (http://creativecommons.org/licenses/by-nc-nd/

4.0/).

#### 1. Introduction

CO<sub>2</sub> flooding is a feasible method for enhanced oil recovery purposes as it can not only provide reservoir energy and enhance oil mobility but also contribute to the reduction of greenhouse gas (Leng et al., 2024). Due to the difference in viscosity and density, the injected CO<sub>2</sub> may preferentially flow towards the production well in a high permeability channel in the reservoir, causing the "fingering" phenomenon and reducing the overall displacement efficiency (Tian et al., 2024). It is proven that the CO<sub>2</sub> water-alternating-gas (CO<sub>2</sub>-WAG) injection can achieve a higher oil recovery when compared with continuous CO<sub>2</sub> injection, which is because the injected water can stabilize the displacement front and expand the

Peer review under the responsibility of China University of Petroleum (Beijing).

swept volume (He et al., 2024.).

Appropriate parameter design for CO<sub>2</sub>-WAG is crucial to realize optimal oil recovery (Chen and Reynolds, 2016) and CO2 storage. CO<sub>2</sub>-WAG, as a typical black-box optimization problem (with only inputs and outputs), is highly compatible with swarm intelligence optimization algorithms. Evolutionary algorithms (Ding et al., 2020; Fonseca et al., 2016; Mohagheghian et al., 2018), e.g., Genetic Algorithm (GA) and Particle Swarm Optimization (PSO), as well as ensemble-based methods (Ma and Leung, 2020) were improved to obtain the optimal well operating parameters, although such a process effectively solves the optimization problem, the efficiency of the optimization is still limited as the original simulation model is computed numerous times. As a result, it requires a significant amount of computational resources, especially at the field scale, to complete the optimization since compositional simulation itself is computationally demanding. To effectively accelerate the process, the original complex simulation model is usually replaced by simpler and faster models during optimization, and such models are termed surrogate models. Two types of surrogate models are commonly implemented, which are physics-

<sup>\*</sup> Corresponding author.

<sup>\*\*</sup> Corresponding author.

*E-mail addresses*: zhangwei93@upc.edu.cn (W. Zhang), yuanbin@upc.edu.cn (B. Yuan).

based surrogates and data-driven surrogates.

The physics-based surrogates, or reduced-order models, use a low-fidelity physics-based simulation model to approximate the original high-fidelity simulation model during the optimization, and this type of surrogate model is generated by simplifying the solution of the original simulation model, and the obtained surrogate model is still based on the solving the mathematical model governing fluid flow. For example, van Doren et al. (2006) applied the Proper Orthogonal Decomposition (POD) technique to reduce the dimension of the discretized governing equations for twophase flow during the water flooding process and constructed a faster surrogate. Cardoso and Durlofsky (2010) further developed a reduced-order modeling technique using the trajectory piecewise linearization method, where the governing equations for twophase flow were linearized before POD procedures. He and Durlofsky (2014) then applied the same technique for the surrogate modeling of compositional simulation. Another physics-based surrogate modeling method is the streamline simulation, which transforms the finite volume solution of a three-dimensional grid system to the finite difference solution along many onedimensional streamlines (Park and Datta-Gupta, 2013; Salehian and Cinar, 2019; Ushmaev et al., 2018). However, the streamline simulation can only be applied to the water flooding process as it cannot treat the nonlinear flow behavior of gas very well. The third physics-based surrogate modeling directly reduces the number of grids of the original simulation model by grid coarsening (Klemetsdal et al., 2019; Lie et al., 2017). The physics-based surrogate modeling can effectively improve computational efficiency. but it may suffer from poor universality.

Instead of the physics-based surrogates, the data-driven approach develops the surrogate model using machine learning models based on data collected from the original simulator. Olalotiti-Lawal et al. (2019) chose the Kriging-based surrogate model and applied the GA to optimize the design parameters for WAG. Bocoum and Rasaei (2023) combined Artificial Neural Networks (ANN) and Nondominated Sorting Genetic Algorithm II (NSGA-II) to optimize cumulative oil recovery and net present value

optimization to accelerate the convergence speed. The reason for this is that the results in the objective function space of the single objective optimization are the endpoints for the Pareto front, as shown in Fig. 1. In addition, in the aspect of the optimization algorithm, the setting of the iteration number for surrogate-modelassisted evolutionary optimization is mostly based on experience. and a reasonable convergence criterion has not vet been provided in the literature to the best of our knowledge, which may lead to unnecessary computational consumption. To fill in this gap, this paper used the single-objective optimization to initialize and accelerate the subsequent multi-objective optimization, meanwhile, a convergence criterion is also proposed based on the analytical characteristics of the surrogate model to further eliminate any redundant computation. This work is built upon a similar method by Liu et al. (2024), in which the single-objective optimization results were not used to initialize the population of the multi-objective optimization. Whereas the algorithm proposed in this work will use the results of single-objective optimization to initialize the population of multiobjective optimization instead of evaluating it through the simulator directly. In addition, the gradient of the surrogate model is used as a criterion to judge the convergence and determine the iteration number instead of embedding it into the meta-heuristic algorithm.

This paper is organized as follows: the next section describes the optimization problem for CO<sub>2</sub>-WAG injection, which is followed by the introduction of our proposed optimization methodology. Then, we apply the methods to two benchmark reservoir simulation examples and compare them with the conventional optimization methods to demonstrate the superiority of the proposed approach. Finally, the conclusions are summarized based on the analysis of the optimization problem.

#### 2. Description of the optimization problem

The goal of  $CO_2$ -WAG is to enhance the oil recovery while storing the  $CO_2$  in the reservoir. Therefore, we choose NPV and  $CO_2$  storage as our optimization objectives. The NPV is defined by Eq. (1):

$$f_1(\mathbf{x}) = \sum_{n=1}^{N_{\rm t}} \left\{ \frac{\Delta t_n}{(1+b)^{\frac{t_n}{360}}} \left[ \sum_{j=1}^{N_{\rm P}} \left( r_{\rm o} \cdot \overline{q_{\rm o,j}^n} - c_{\rm w} \cdot \overline{q_{\rm w,j}^n} \right) - \sum_{k=1}^{N_{\rm t}} \left( c_{\rm wi} \cdot \overline{q_{\rm wi,k}^n} + c_{\rm gi} \cdot \overline{q_{\rm gi,k}^n} \right) \right] \right\}, \tag{1}$$

(NPV). Nait-Amar et al. (2021) combined the multi-layer perceptron model and Radial Basis Function (RBF) with metaheuristic algorithms to build the surrogate model for WAG simulation. Ding et al. (2022) used multi-objective PSO (MOPSO) to maximize cumulative oil production and CO<sub>2</sub> storage in low permeability reservoirs for WAG. Enab and Ertekin (2021) proposed a reliable ANN to predict, optimize, and history match the process of WAG. Agada et al. (2016) used polynomial regression and polynomial chaos expansion to decrease the computational consumption and employed GA to optimize the parameters of WAG. The above implementation of machine-learning surrogate models showed a more significant reduction in optimization.

A growing body of literature can be found on the surrogate-assisted single-objective optimization and multi-objective optimization. However, the combination of single-objective optimization and multi-objective optimization has been paid less attention. In this work, we leveraged the results of single-objective optimization as prior knowledge to initialize the population for multi-objective

where  $\mathbf{x}$  is a N-dimensional column vector which contains all optimization variables; n denotes the nth timestep of the reservoir simulation;  $N_{\rm t}$  is the total number of timestep;  $t_n$  denotes the time at the end of the nth timestep; b is the annual discount rate;  $N_{\rm P}$  and  $N_{\rm I}$  are the number of producers and injectors, respectively;  $r_{\rm o}$ ,  $c_{\rm w}$ ,  $c_{\rm wi}$ , and  $c_{\rm gi}$  denote the oil revenue, the disposal cost of produced water, the cost of water injection, and the cost of gas injection, USD/m³;  $\overline{q}_{\rm o,j}^n$  and  $\overline{q}_{\rm wi,j}^n$  denote the jth production well's average oil production rate at jth timestep, respectively, j0, j1, j2, j3, j4, j5, j6, j8, j9, j9,

The amount of  $CO_2$  storage can be calculated by Eq. (2):

$$f_2(x) = m_{\rm str} + m_{\rm res} + m_{\rm sol} + m_{\rm min},$$
 (2)

where  $m_{\text{str}}$  denotes the amount of CO<sub>2</sub> for structural trapping;  $m_{\text{res}}$  denotes the amount of CO<sub>2</sub> for residual trapping;  $m_{\text{sol}}$  denotes the

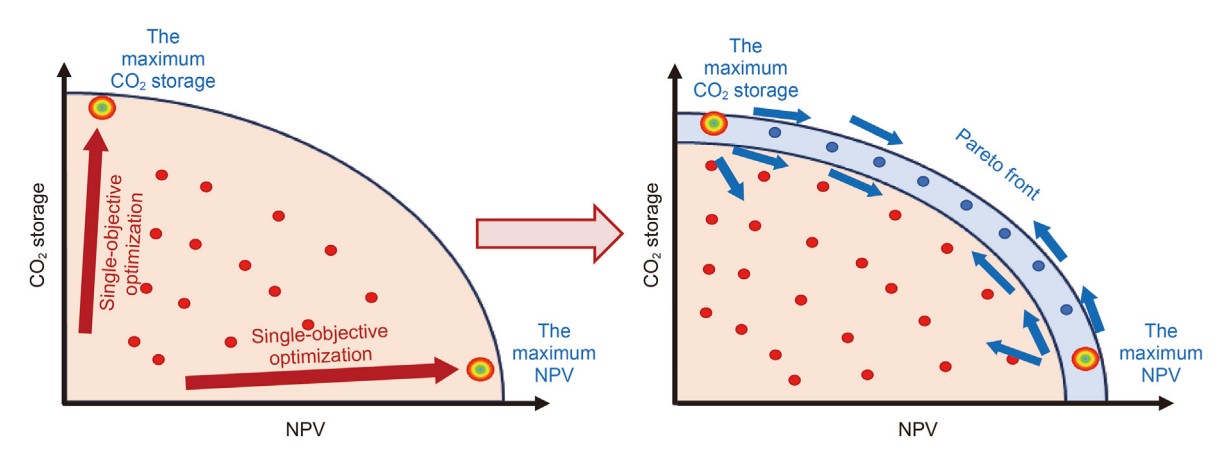


Fig. 1. The relationship between the results of single-objective optimization and Pareto front endpoints.

amount of  $CO_2$  for solubility trapping;  $m_{\min}$  denotes the amount of  $CO_2$  for mineral trapping. The unit of the above variables is in kg. The specific value of the above variables at each timestep can be obtained from the CMG result files (CMG, 2023).

Considering the above two objectives, the multi-objective optimization problem for CO<sub>2</sub>-WAG can be defined by Eq. (3):

$$\begin{cases} \operatorname{Max} f(\mathbf{x}) = [f_1(\mathbf{x}), f_2(\mathbf{x})], \\ s.t. \, \mathbf{x}_i^{\text{low}} \le \mathbf{x}_i \le \mathbf{x}_i^{\text{up}}, \ i = 1, 2, 3, ..., N_u \end{cases}$$
 (3)

In fact, the relation of two objective functions is not known in advance. Thus, we adopt the concept of "Pareto Optimality". To better understand the concept, we provide the following definitions for Pareto optimal points: a vector  $\mathbf{p}=(a_1, a_2, ..., a_m)$  and another vector  $\mathbf{q}=(b_1, b_2, ..., b_m)$  are two solutions of multiobjective optimization, if  $f_i(\mathbf{q}) \leq f_i(\mathbf{p})$  for  $\forall i=1, 2$  and  $f_j(\mathbf{q}) < f_j(\mathbf{p})$  for at least one j value (j=1, 2),  $\mathbf{p}$  is said to dominate  $\mathbf{q}$ . The set of all Pareto solutions is named Pareto set (PS) in the decision space. The set of PS in the objective space is called the Pareto front (PF).

### 3. Optimization methodology

To eliminate the influence of dimensions, the dataset was normalized when training the surrogate model: the maximum and the minimum values of CO<sub>2</sub> storage and NPV in the dataset are used to normalize the objective functions, and the optimization parameters are normalized by their respective upper and lower limits. The surrogate model adopted by this paper is RBF, which is more suitable for high-dimensional interpolation. It can be expressed as Eq. (4):

$$f(\mathbf{x}) = p(\mathbf{x})w_p + \sum_{i=1}^{nt} \emptyset(\mathbf{x}, \mathbf{x}_{ti})w_r,$$
(4)

where  $\mathbf{x}$  is the input vector;  $f(\mathbf{x})$  is the model output;  $p(\mathbf{x})$  is polynomial;  $w_p$  is the weight for  $p(\mathbf{x})$ ; nt is the number of training points;  $\mathbf{x}_{ti}$  is the ith training point;  $w_r$  is the weight for  $\emptyset$ ;  $\emptyset$  is the radial basis function, it is given by Eq. (5):

$$\varnothing(\boldsymbol{x},\,\boldsymbol{y}) = e^{-\left(\frac{\|\boldsymbol{x}-\boldsymbol{y}\|_2}{d_0^2}\right)},\tag{5}$$

where  $d_0$  is a hyperparameter.  $w_p$  and  $w_r$  can be obtained by Eq. (6):

$$\begin{bmatrix} \varnothing(\mathbf{x}_{t1}, \mathbf{x}_{t1}) & \dots & \varnothing(\mathbf{x}_{t1}, \mathbf{x}_{tnt}) & p(\mathbf{x}_{t1}) \\ \vdots & \ddots & \vdots & & \vdots \\ \varnothing(\mathbf{x}_{tnt}, \mathbf{x}_{t1}) & \dots & \varnothing(\mathbf{x}_{tnt}, \mathbf{x}_{tnt}) & p(\mathbf{x}_{tnt}) \\ p(\mathbf{x}_{t1}) & \dots & p(\mathbf{x}_{tnt}) & 0 \end{bmatrix} \begin{bmatrix} w_{r1} \\ \vdots \\ w_{rnt} \\ w_{p} \end{bmatrix} = \begin{bmatrix} y_{t1} \\ \vdots \\ y_{tnt} \\ 0 \end{bmatrix},$$
(6)

where  $y_{ti}$  is the output of the *i*th training points;  $p(\mathbf{x})$  is constant in this paper.

Most of the multi-objective optimization algorithms overlooked the endpoints of the Pareto front. The Multi-objective Evolutionary Algorithm based on Decomposition (MOEA/D) noticed the endpoints of the Pareto front, but it cannot select the most reasonable decomposition method in advance for a practical problem. Thus the optimization algorithms adopted by this paper are Differential Evolution (DE) (Storn and Price, 1997) and NSGA-II (Deb et al., 2002). As mentioned in the previous sections, this study combines single-objective optimization with multi-objective optimization to accelerate the computation, and the DE algorithm is used to perform the single-objective optimization while the NSGA-II is adopted for multi-objective optimization. The specific steps of DE and NSGA-II are shown in Tables 1 and 2.

This study uses the DE algorithm to perform single-objective optimization to get the maximum NPV and the maximum CO<sub>2</sub> storage on the surrogate models, respectively. The extreme values of the two individual objectives obtained through single-objective optimization are the endpoints of the Pareto front, which is the final set of solutions for multi-objective optimization. Therefore, we add the corresponding optimum of each single objective as prior knowledge to the initial population of multi-objective optimization, so that the moving speed of the population towards the Pareto front during multi-objective optimization can be significantly enhanced. In addition, we propose the following convergence criterion to further accelerate single-objective pre-search.

By definition, the multi-variable gradient of the optimal solution can be expressed as Eq. (7):

$$\operatorname{grad}(\mathbf{x}) = \left(\frac{\partial f}{\partial x_1} \quad \frac{\partial f}{\partial x_2} \quad \dots \quad \frac{\partial f}{\partial x_n}\right). \tag{7}$$

The global optimum solution in single-objective optimization exhibits two distinct characteristics: either the gradient components at the optimum approach zero, or the design variables reside at constraint boundaries. To mitigate interference from local optima (identified by normalized surrogate model values below 1),

#### Table 1

The procedure of DE algorithm.

The steps of DE

Step 1: Initialize the population,  $\mathbf{x} = \mathbf{x}_{low} + rand \times (\mathbf{x}_{up} - \mathbf{x}_{low}), rand \in [0, 1]$ 

Step 2: Mutation (DE/rand/1),  $\mathbf{v}_{i,G} = \mathbf{x}_{r_1,G} + F \times (\mathbf{x}_{r_2,G} - \mathbf{x}_{r_3,G})$ ,  $\mathbf{x}_{r_1,G}$ ,  $\mathbf{x}_{r_2,G}$ , and  $\mathbf{x}_{r_3,G}$  are three randomly selected individuals in Gth generation, F is the mutation factor,  $\mathbf{v}_{i,G}$  is the new individual generated by mutation.

Step 3: Crossover,  $\mathbf{u}_{j,i,G} = \begin{cases} \mathbf{v}_{j,i,G} & \text{rand} \leq CR \text{ or } j = j_{\text{rand}} \\ \mathbf{x}_{j,i,G} & \text{other} \end{cases}$ , CR is the crossover probability,  $\mathbf{x}_{j,i,G}$  denotes the jth variable of ith individual in Gth generation,  $j_{\text{rand}}$  is a random integer ranging from 1 to the variable dimension.

Step 4: Selection,  $\mathbf{x}_{i,G+1} = \begin{cases} \mathbf{u}_{i,G} \text{ if } f(\mathbf{u}_{i,G}) > f(\mathbf{x}_{i,G}) \\ \mathbf{x}_{i,G} \end{cases}$ 

Step 5: Judge whether the maximum number of iterations is met. If the maximum number of iterations is reached, then cease iteration and add the optimal individuals corresponding to the optimal values to the initial population of the subsequent multi-objective optimization. Otherwise, G = G + 1 and return to Step 2.

**Table 2**The procedure of NSGA-II algorithm.

The steps of NSGA-II

Step 1-Step 3 are the same as DE.

Step 4: Perform fast non-dominated sorting on the population, compute the crowding distance for each individual, and subsequently select the most competitive candidates to generate a new population.

Step 5: Judge whether the maximum number of iterations is met. If the maximum number of iterations is reached, then cease iteration and use the numerical simulator to simulate the optimal case obtained in the iterations. Otherwise, G = G + 1, and return to Step 2.

we impose an additional criterion requiring predicted objective function values on the surrogate model to exceed 1. This threshold ensures selected solutions surpass the current best performance on the surrogate model, as illustrated in Fig. 2. While this approach retains a non-zero probability of converging to local extrema, Eq. (8) shows that the local optimum still remains advantageous for initializing populations in multi-objective optimization

$$\begin{cases} u = ||w \cdot \mathbf{grad} 1 + (1 - w) \cdot \mathbf{grad} 2||_2 \cdot = 0 \\ w = \operatorname{argmin}(u) \\ 0 < w < 1 \end{cases}$$
 (8)

where **grad**1 and **grad**2 are the gradients of two objective functions; w is a weight parameter. For example, even if a local optimum solution of NPV is reached, then its corresponding gradient **grad**1 is a zero vector, then u will be zero when w is equal to 1. This means it

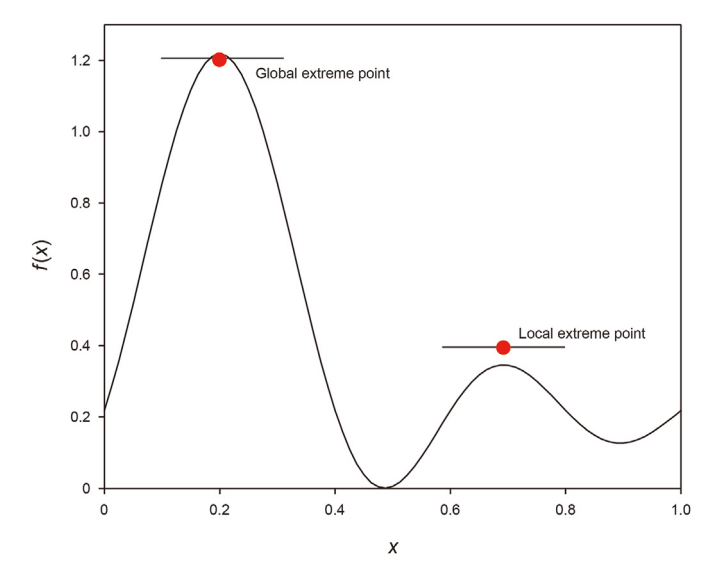


**Fig. 2.** The illustration of the convergence criterion.

is a Pareto-stationary design-point, which is much better than a solution generated randomly to initialize the population of multiobjective optimization.

During the single-objective pre-search, the convergence criterion is not checked in each iteration. We will first check the convergence criterion after some certain iteration numbers  $(k_1)$ , if the criterion is met at this iteration, then the iteration will be stopped. Otherwise, the iteration will continue and the convergence criterion will be checked every  $k_2$  iterations until the criterion is met. For example,  $k_1 = 500$  and  $k_2 = 100$  means the criterion will be checked at the 500th, 600th, 700th iteration step and so on, until the described criterion is satisfied, as shown in Fig. 3. The overall optimization workflow of this work can be shown in Fig. 4.

#### 4. Case study

**Case 1.** The reservoir model is a modified "Egg" model (Jansen et al., 2014). The geological parameters and well-location parameters are the same as the original "Egg" model, as shown in Fig. 5. The model has a  $60 \times 60 \times 7$  grid system with dimensions  $12 \text{ m} \times 12 \text{ m} \times 4 \text{ m}$ . The relative permeability curves are shown in Fig. 6. The porosity is a constant of 0.2. The compositional model considers 5 components, which are  $N_2$  to  $C_1$ , i- $C_4$  to n- $C_5$ ,  $C_2$ ,  $C_2$  to  $C_3$ , and  $C_6$  to  $C_9$ . The binary interaction coefficients, properties, and initial conditions of the components are shown in Tables 3—5, while

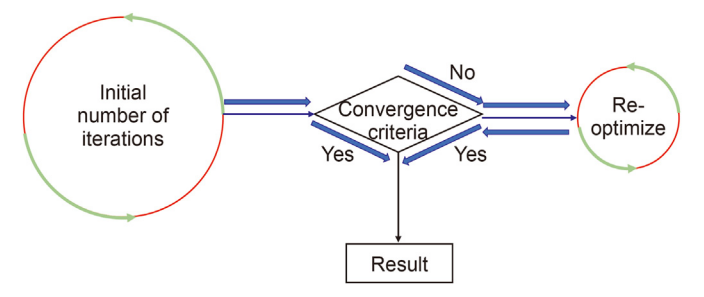


Fig. 3. The optimization based on the convergence criterion.

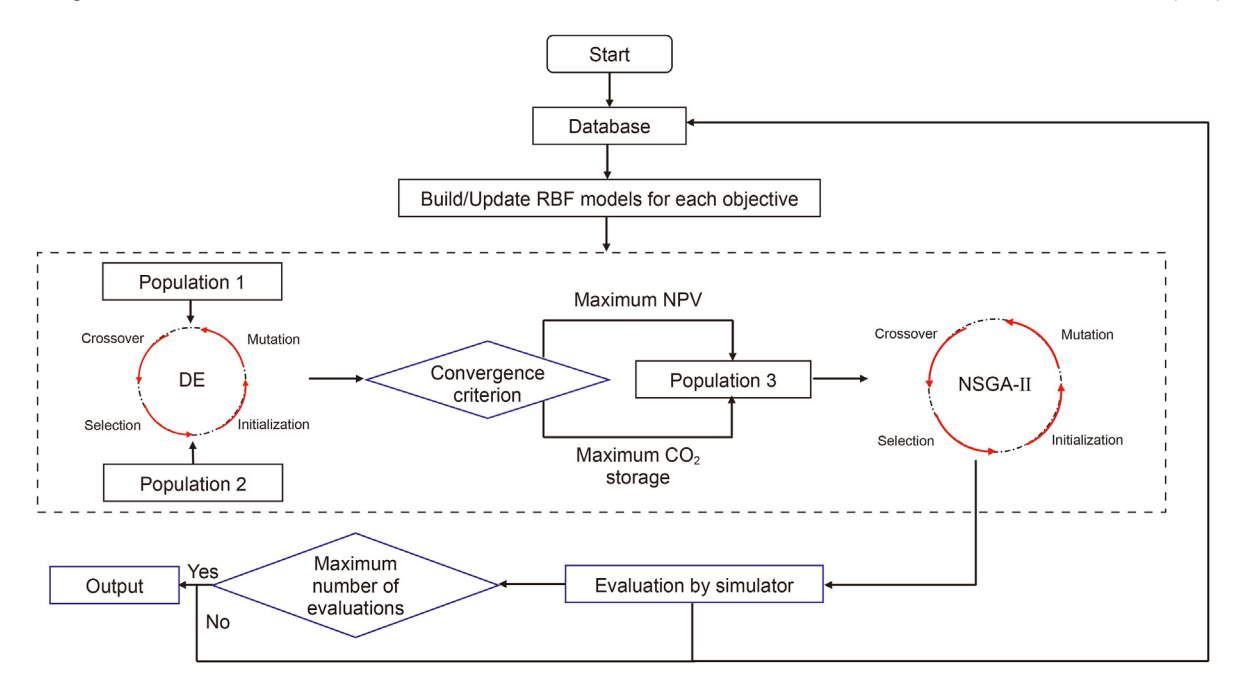


Fig. 4. The overall workflow of the proposed optimization method.

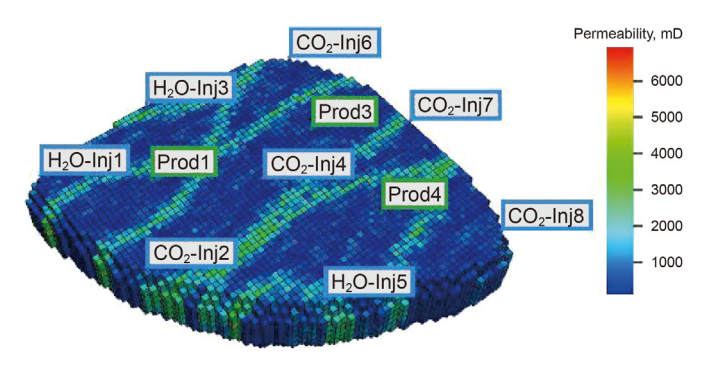


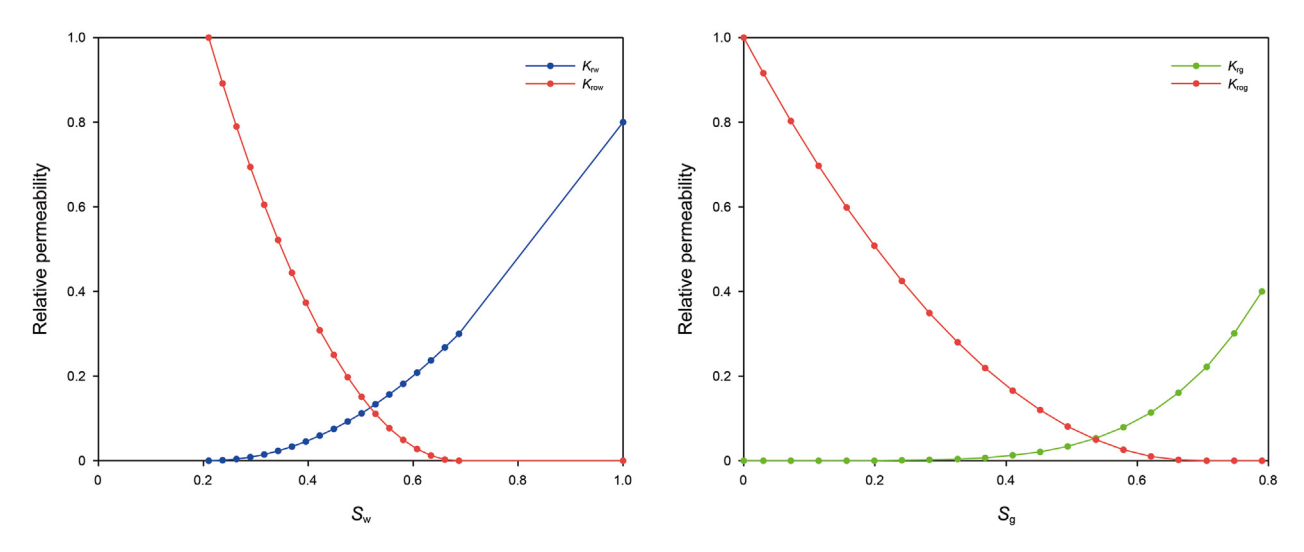
Fig. 5. The modified Egg model.

Table 6 presents the considered chemical reaction equations. The initial pressure of the reservoir is 40 MPa. The production time is

**Table 3**The binary interaction coefficients between the considered components of the Egg model.

	N <sub>2</sub> -C <sub>1</sub>	CO <sub>2</sub>	C <sub>2</sub> -C <sub>3</sub>	i-C <sub>4</sub> -n-C <sub>5</sub>	C <sub>6</sub> -C <sub>9</sub>
N <sub>2</sub> -C <sub>1</sub>	0.000	0.130	0.008	0.021	0.045
$CO_2$	0.130	0.000	0.135	0.125	0.101
$C_2-C_3$	0.008	0.135	0.000	0.003	0.016
$i-C_4-n-C_5$	0.021	0.125	0.003	0.000	0.005
C <sub>6</sub> -C <sub>9</sub>	0.045	0.101	0.016	0.005	0.000

1800 d, and the design variables are shown in Table 7. In each cycle, we adjust the half-cycle durations for different injectors. The specific approach is to calculate the time points at which the injectors transition from water to gas injection, and write the production operation to the data file in chronological order after sorting these time points. The described optimization problem results in 160 optimization variables. It is worth noting that the lower bounds of



 $\textbf{Fig. 6.} \ \ \textbf{The relative permeability curves.}$ 

**Table 4**The component properties of the Egg model.

	Critical pressure, atm	Critical temperature, K	Acentric factor	$\Omega_{A}$	$\Omega_{\mathrm{B}}$
N <sub>2</sub> -C <sub>1</sub>	43.60	180.02	0.01	0.46	0.08
$CO_2$	72.80	304.20	0.23	0.37	0.06
$C_2-C_3$	44.08	350.22	0.13	0.46	0.08
$i-C_4-n-C_5$	35.37	442.26	0.21	0.46	0.08
C <sub>6</sub> -C <sub>9</sub>	27.60	592.91	0.33	0.46	0.08

**Table 5**The initial compositional of each component.

Component name	$N_2-C_1$	CO <sub>2</sub>	$C_2 - C_3$	i-C <sub>4</sub> -n-C <sub>5</sub>	$C_6 - C_9$
Proportion	0.0549627	0.0034125	0.0977151	0.127606	0.299294

**Table 6** The considered chemical reaction equations.

Chemical reaction equation	
$CO_2 + H_2O = H^+ + HCO_3^-$	
$Calcite + H^{+} = Ca^{2+} + HCO_{3}^{-}$	

**Table 7** Design variables of the Egg model.

Design variable	Upper bound	Lower bound
Water injection rate, m <sup>3</sup> /d	180	0
Gas injection rate, m <sup>3</sup> /d	30000	0
BHP of the producer, kPa	39500	32500
Half-cycle duration, d	360	0

Note: Half-cycle duration is the water injection time in a  ${\rm CO_2\text{-}WAG}$  cycle.

the water injection rate, gas injection rate, and half-cycle are set as 0, which can ensure that water flooding and continuous gas injection are included and the duration of the  $\rm CO_2$ -WAG cycle is more flexible. When the half-cycle is set to 0 or 360, the setting of the gas injection rate or water injection rate is invalid, which will cause different injection schemes to correspond to the same objective value, which is disadvantageous for the optimization. To deal with this, we forcefully set the water injection or the gas injection rate to 0 when the half-cycle is equal to 0 or 360.

The simulator employed in the simulation is the GEM of CMG 2022 and the economic parameters are given in Table 8. Sensitivity analysis, as shown in Table 9, was performed before optimization to understand the influence of different optimization variables on the objective functions. The results show that the NPV will increase due to the increase in water injection rate, but the cumulative  $CO_2$  storage will decrease when water flooding is incorporated. The NPV and cumulative  $CO_2$  storage will increase when the gas injection rate increases, when considering continuous gas injection, but the NPV under the maximum gas injection rate is less than the NPV under the maximum water injection rate, which may be due to gravitational differentiation. An increase in half-cycle duration will increase the NPV and decrease  $CO_2$  storage. In contrast, an increment of bottomhole pressure will reduce the NPV but enhance the cumulative  $CO_2$  storage.

As for the setting of the algorithm parameter, the hyperparameter  $d_0$  of the RBF model is 5, the mutation factor is 0.5, the crossover probability is 0.7, the population size of DE is 50, the initial iteration number is  $k_1 = 500$ , and the convergence will be checked for every 100 iteration steps if convergence is not satisfied ( $k_2$  = 100). For the multi-objective optimization, the mutation factor and crossover probability of NSGA-II are the same as the DE, the population of the NSGA-II is 10, and the initial iteration number is 1000. For the convergence criterion, we define the single-objective optimization converges on the surrogate model when the value of the gradient component is less than 0.001 or when the distance between the optimization variable and the boundary is less than 0.001. The initial number of samples is 100. The sampling process initiates with Latin Hypercube Sampling (LHS), a space-filling technique particularly effective for high-dimensional parameter spaces, to generate representative initial sample points. These sampled values are subsequently mapped into the constrained domain of optimization variables based on predetermined upper and lower bounds. Ultimately, this procedure establishes a comprehensive dataset that systematically correlates production scheme parameters with their associated objective function values. The maximum evaluation times for the simulator is 200.

To show the superiority of the proposed algorithm (RBF-DE-NSGA-II-C), we compare it with the algorithm without singleobjective pre-search or convergence criterion (RBF-NSGA-II), the algorithm with pre-search but without convergence criterion (RBF-DE-NSGA-II), and the algorithm by Zhao et al. (2020) (PCA-K-RVEA). To ensure fairness of comparison, the parameter settings of all compared algorithms are set to be the same. As our proposed methodology includes pre-search by single-objective optimization, we record the total number of surrogate model evaluations of our algorithm and set the overall iteration number of all three compared algorithms to be the same, which is 11500. This means that the total iteration steps consumed by single-objective and multi-objective optimizations is 11500 for our proposed algorithm, and the other three algorithms (RBF-NSGA-II, RBF-DE-NSGA-II, and PCA-K-RVEA) also used totally 11500 iteration steps to perform the optimizations. The maximum number of evaluations for the numerical simulator is 200 for all four compared algorithms.

The optimization results are shown in Fig. 7, the optimization consumed 669 min with 11th Gen Intel® Core i7-11700 @ 2.50 GHz. We can find the Pareto front obtained by our algorithm, after the validation of the numerical simulator, is obviously the highest among all the four algorithms, which means it outperforms the three other algorithms with the same computational cost. The presearch and appropriate iteration in each cycle resulted in its superiority. The comparison of points  $A_1$ ,  $A_2$ ,  $A_3$ ,  $A_4$  and  $B_1$ ,  $B_2$ ,  $B_3$ ,  $B_4$  are shown in Figs. 8 and 9. For the first group ( $A_1$ ,  $A_2$ ,

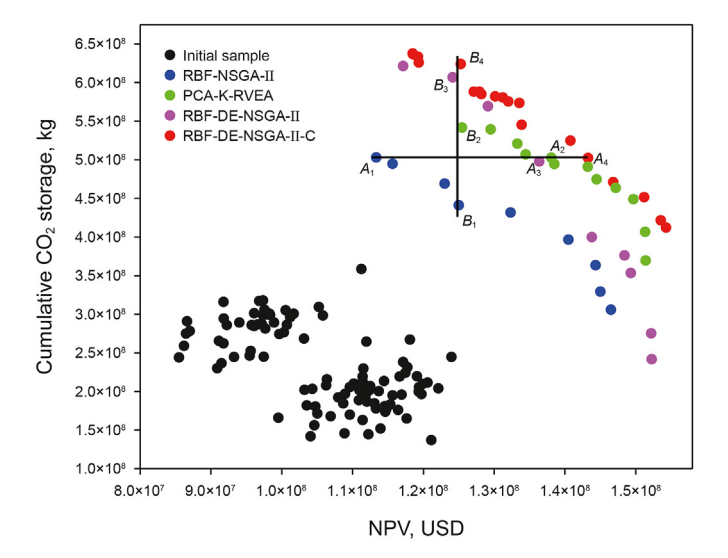
**Table 8**The economic parameters (Botechia et al., 2023).

Oil price, USD/m <sup>3</sup>	Water-injection cost, USD/m <sup>3</sup>	Gas-injection cost, USD/m <sup>3</sup>	Water disposal cost, USD/m <sup>3</sup>	Producer gas disposal cost, $USD/m^3$	Annual discount rate
314.5	4.65	0.0134	4.65	0.0124	0.09

R.-F. Yang, W. Zhang, S.-C. Liu et al. Petroleum Science 22 (2025) 2967–2976

**Table 9**The sensitivity analysis of the Egg model.

Experiment No.	Half-cycle, d	Water injection rate, m <sup>3</sup> /d	Gas injection rate, m <sup>3</sup> /d	BHP of the producer, kPa	NPV, USD	Cumulative CO <sub>2</sub> storage, kg
1	360	60	0	32500	98918623.2	2992916.0
2	360	120	0	32500	127738171.2	2289048.0
3	360	180	0	32500	139900157.6	1793167.0
4	0	0	10000	32500	51299460.6	250903300.0
5	0	0	20000	32500	83204630.1	436071700.0
6	0	0	30000	32500	105749417.1	579029800.0
7	90	60	10000	32500	73964257.0	197345000.0
8	180	60	10000	32500	86323988.0	134306900.0
9	270	60	10000	32500	93939899.4	68863020.0
10	270	120	20000	34500	92288663.4	68893720.0
11	270	120	20000	36500	90722856.6	68971060.0
12	270	120	20000	38500	88762706.6	68977090.0



 $\textbf{Fig. 7.} \ \ \textbf{The optimization results under different algorithms.}$ 

 $A_3$ ,  $A_4$ ), their cumulative  $CO_2$  storage is almost equal, but the cumulative oil production of the proposed algorithm is the highest and the cumulative water production is relatively lower under the production scheme obtained by RBF-DE-NSGA-II-C. The production schemes in the second group  $(B_1, B_2, B_3, B_4)$  return almost the same NPV, but the cumulative  $CO_2$  storage of " $B_4$ " is the greatest.

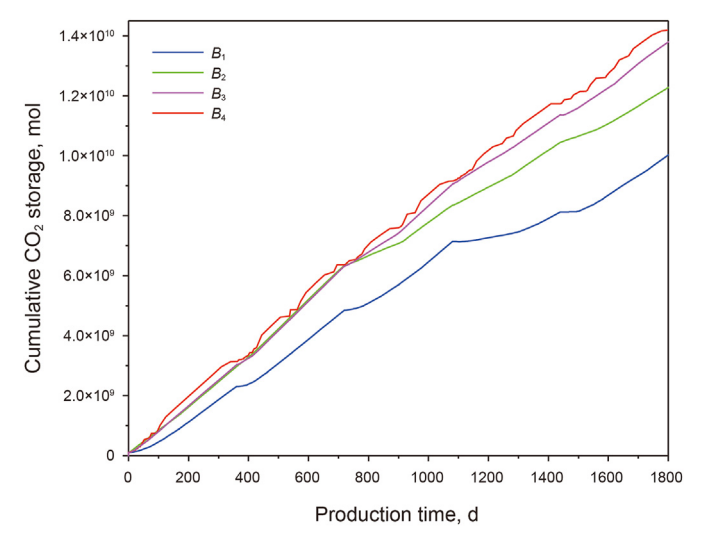
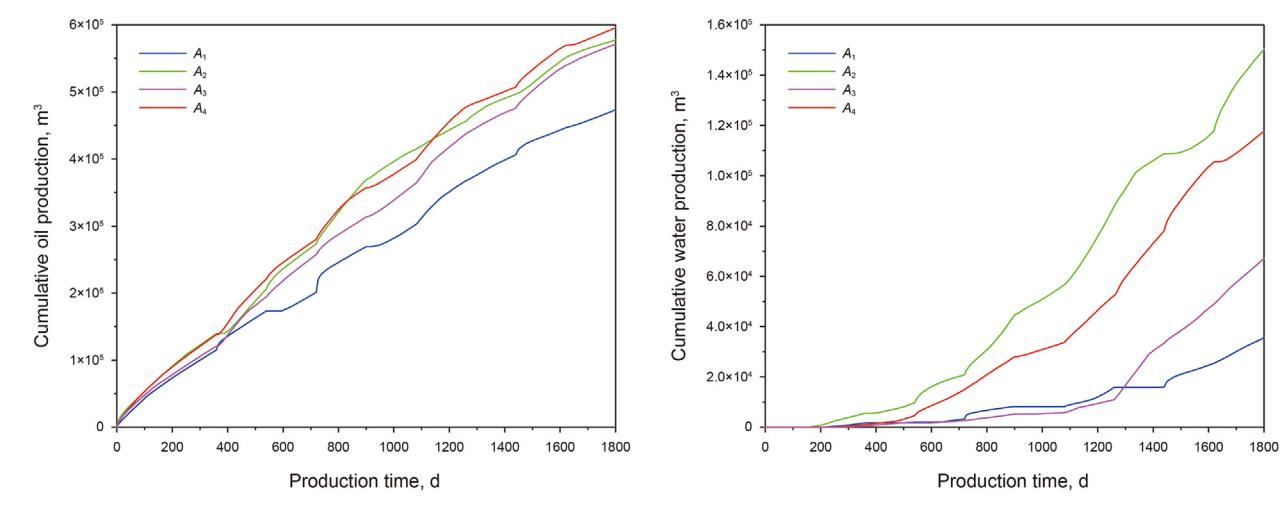


Fig. 9. The cumulative  $CO_2$  storage at points  $B_1$ ,  $B_2$ ,  $B_3$ , and  $B_4$ .

**Case 2.** The reservoir model is also a benchmark simulation model (the 'Cap' model) modified from Afanasyev and Vedeneeva (2021). The reservoir model and its initial oil saturation are shown in Fig. 10. The relative permeability curves and components are the same as those in the "Egg" model of Case 1. The considered chemical reaction equations are in Table 10. The initial pressure of the reservoir is 24 MPa and the production time is 1800 d. The



**Fig. 8.** The cumulative oil and water production at points  $A_1$ ,  $A_2$ ,  $A_3$ , and  $A_4$ .

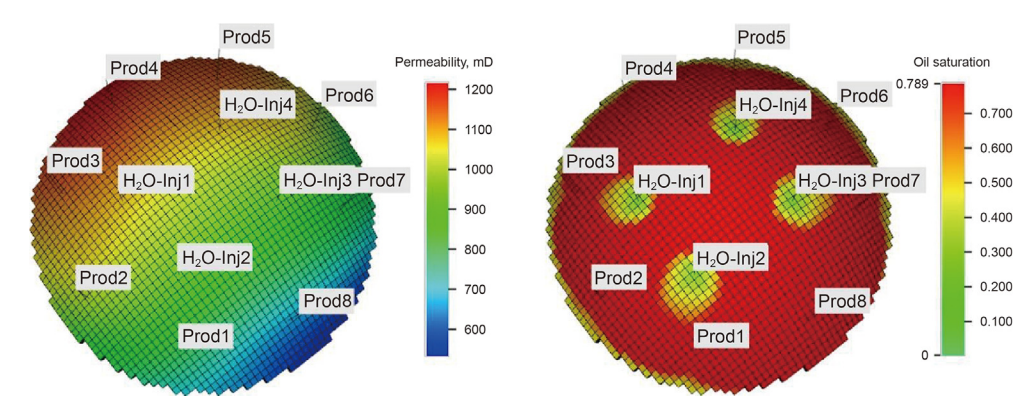


Fig. 10. The reservoir model and its initial oil saturation.

**Table 10**The considered chemical reaction equations.

Chemical reaction equation	
$H^+ + OH^- = H_2O$	
$CO_2 + H_2O = H^+ + HCO_3^-$	
$CO_3^{2-} + H^+ = HCO_3^-$	
$Kaolinit + 6H^+ = 5H_2O + 2Al^{3+} + 2SiO_2(aq)$	
$Anorthit + 8H^+  = 4H_2O + Ca^{2+} + 2Al^{3+} + 2SiO_2(aq)$	

**Table 11**The design variable of the reservoir model

Design variable	Upper bound	Lower bound	
Water injection rate, m³/d	250	0	
Gas injection rate, m³/d	18000	0	
BHP of the producer, kPa	10000	5000	
Half-cycle duration, d	360	0	

Note: half-cycle duration is the water injection time in a  ${\rm CO_2\text{-}WAG}$  cycle.

design variables are shown in Table 11 and the total number of optimization variables is 140. With the same economic parameters shown in Case 1, a sensitivity analysis was also performed for Case 2, and the results are shown in Table 12. It can be found that the trend of the objective functions is the same as Case 1.

Similarly, the parameter settings of the algorithms are the same as those in Case 1. The optimization for Case 2 consumed 593 min with 11th Gen Intel® Core i7-11700 @ 2.50 GHz. Obviously, it can be found in Fig. 11 that the proposed algorithm gives the best outcome within the same iteration number, which means that the prior knowledge by the single-objective optimization and the convergence criterion both worked well. The prior knowledge explores the

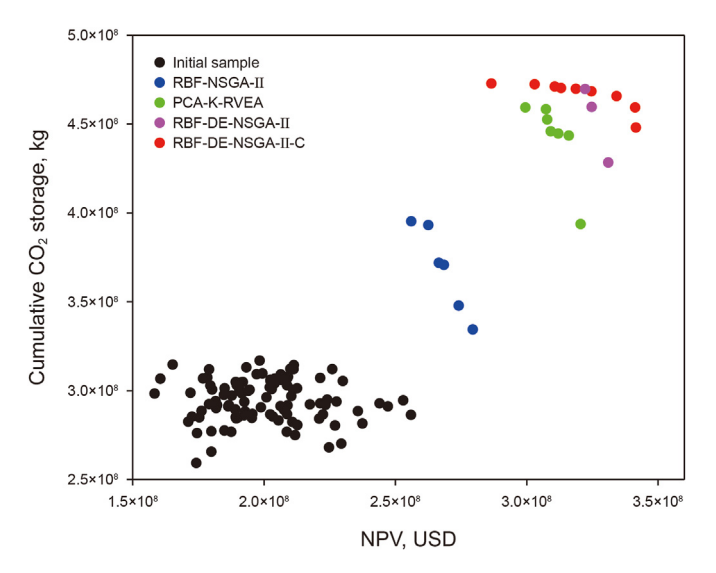
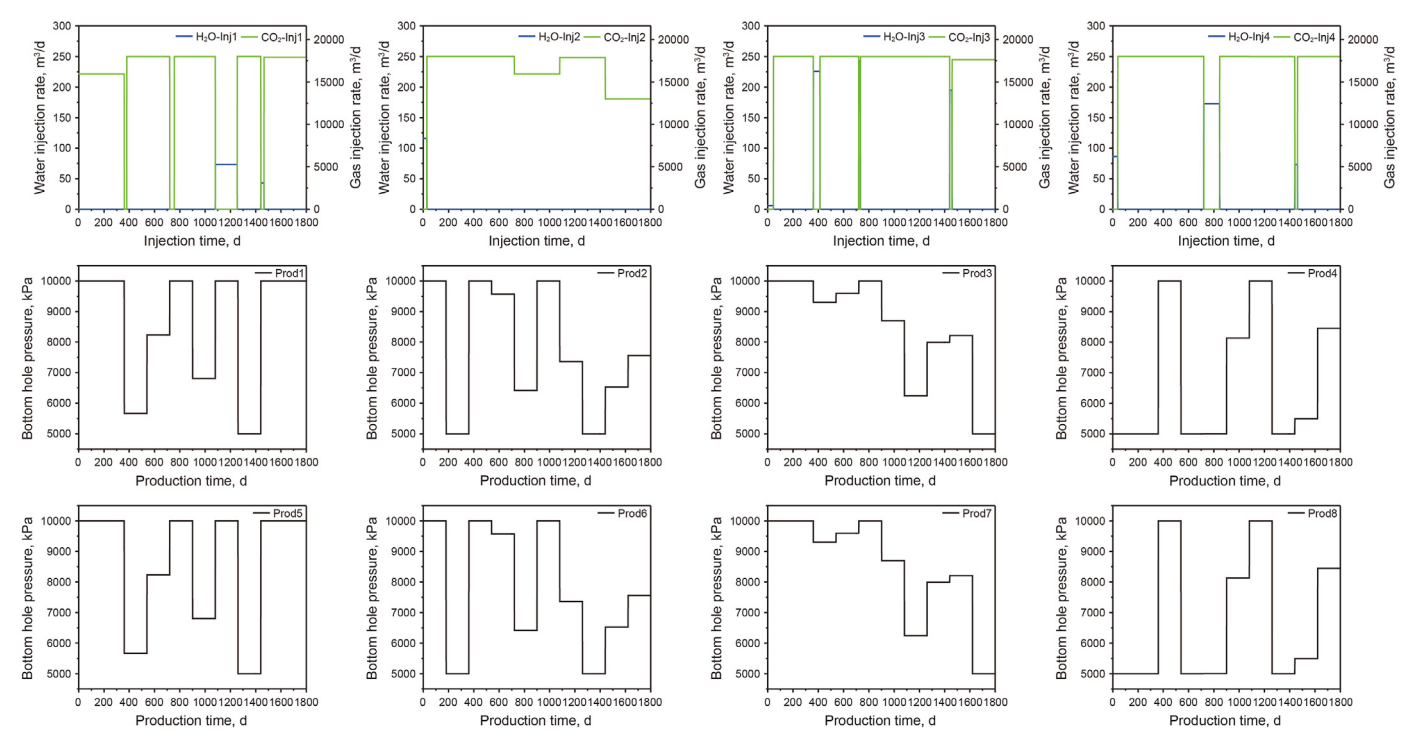


Fig. 11. The optimization results under different algorithms.

endpoints of the Pareto front, while the convergence criterion ensures a full search on the surrogate model. The production scheme under the maximum NPV obtained by our algorithm is shown in Fig. 12. The distribution of CO<sub>2</sub> and relative ions corresponding to the maximum NPV case is shown in Fig. 13. It can be found that CO<sub>2</sub> is mainly distributed around the wells, and the injected CO<sub>2</sub> almost achieved uniform flooding with the optimized well schedules. Fig. 14 shows the proportion of different trapping mechanisms under the maximum CO<sub>2</sub> storage, and the amount of CO<sub>2</sub> storage due to structural trapping accounts for half of the total CO<sub>2</sub> storage.

**Table 12**The sensitivity analysis of the reservoir model.

Experiment No.	Half-cycle, d	Water injection rate, m <sup>3</sup> /d	Gas injection rate, m <sup>3</sup> /d	BHP of the producer, kPa	NPV, USD	Cumulative CO <sub>2</sub> storage, kg
1	360	150	0	5000	249466952.8	232975900.0
2	360	200	0	5000	268415980.3	231645600.0
3	360	250	0	5000	287128766.6	230325600.0
4	0	0	6000	5000	218756939.7	315467800.0
5	0	0	12000	5000	252490050.2	393385400.0
6	0	0	18000	5000	283760177.7	471382900.0
7	90	200	12000	5000	253544151.7	353016500.0
8	180	200	12000	5000	255231294.7	312951100.0
9	270	200	12000	5000	260171887.0	272527000.0
10	270	200	12000	6500	233078695.3	273760400.0
11	270	200	12000	8000	210388960.4	274312200.0
12	270	200	12000	9500	190609304.4	275169700.0



**Fig. 12.** The production scheme under the maximum NPV.

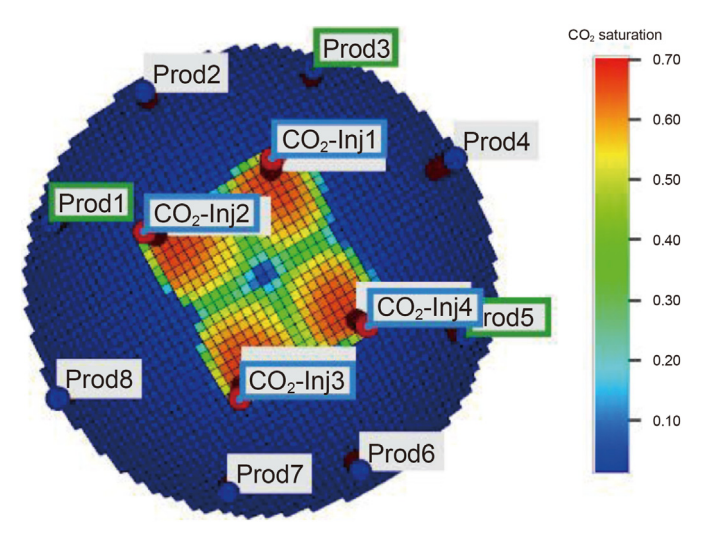


Fig. 13. The distribution of CO<sub>2</sub> in Case 2.

For both the Egg model (Case 1) and Cap model (Case 2), we use the hypervolume value (HV) (Guerreiro et al., 2021) to measure the performance of different algorithms quantitatively, and the reference point is set to be (0, 0). A higher HV value usually indicates a higher optimization efficiency. From Table 13, it can be found that the HV of the proposed algorithm achieved the largest value in the two benchmark models. The effect of single-objective pre-search can be demonstrated by the performance comparison between RBF-DE-NSGA-II and RBF-NSGA-II, the HV value is significantly improved by approximately 59.7% and 194.3% in Case 1 and Case 2, respectively. The effect of the convergence criterion can be demonstrated by the performance comparison between RBF-DE-NSGA-II-C and RBF-DE-NSGA-II, and it is shown that the convergence criterion further enhanced the HV value by 31.2% and 9.98%.

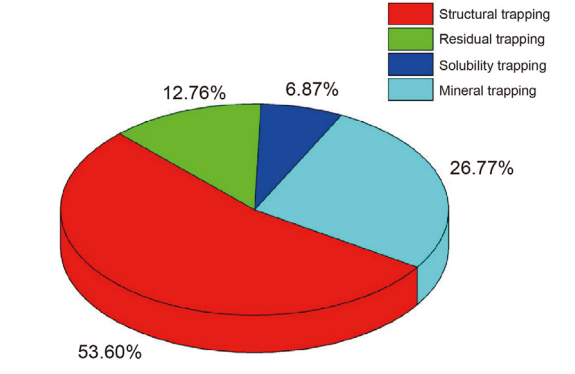


Fig. 14. The proportion of different trapping mechanisms under the maximum  ${\rm CO}_2$  storage case.

**Table 13**The HV value of different algorithms on two reservoir models.

Algorithm	Case 1	Case 2
RBF-NSGA-II (with 11500 iterations)	0.3660	0.3061
RBF-NSGA-II (with 12500 iterations)	0.6081	0.1846
PCA-K-RVEA (with 11500 iterations)	0.6247	0.7774
PCA-K-RVEA (with 12500 iterations)	0.5906	0.8778
RBF-DE-NSGA-II (with 11500 iterations)	0.5845	0.9010
RBF-DE-NSGA-II-C (with 11500 iterations)	0.7671	0.9910

For RBF-NSGA-II and PCA-K-RVEA, the iteration number is increased to 12500 to check if the HV value would be improved with more iterations, but it can be found that an increase in iteration number does not guarantee HV improvement. For Case 1, the HV of RBF-NSGA-II is enhanced while the HV of PCA-K-RVEA is reduced. For Case 2, the results are completely the opposite. The proposed algorithm still outperforms these two algorithms with more iterations in terms of HV.

#### 5. Conclusions

This study develops an integrated multi-objective optimization framework for CO<sub>2</sub> water-alternating-gas (WAG) and CO<sub>2</sub> flooding processes. Through treating single-objective optimization results as prior knowledge for population initialization, as well as establishing an adaptive convergence criterion to determine optimal iteration thresholds for preliminary single-objective searching, the subsequent multi-objective is significantly accelerated. The investigation of this work yields two principal findings.

- (1) Strategic incorporation of single-objective optimization outcomes into multi-objective population initialization substantially accelerates Pareto front convergence rates. Computational experiments demonstrate that this presearch mechanism enhances optimization efficiency by 59% compared to conventional initialization approaches.
- (2) The establishment of convergence criterion can help determining the number of iterations for the single-objective presearch. It can avoid the empirical setting of the iteration number for the single-objective optimization. Implementation of this criterion achieves a 9.98% improvement in hypervolume (HV) indicator for the overall optimization workflow.

#### **CRediT authorship contribution statement**

**Ren-Feng Yang:** Software, Resources, Project administration, Methodology, Funding acquisition, Data curation. **Wei Zhang:** Writing — review & editing, Validation, Resources, Methodology, Funding acquisition, Data curation, Conceptualization. **Shuai-Chen Liu:** Writing — original draft, Visualization, Validation, Software. **Bin Yuan:** Validation, Supervision, Software, Resources. **Wen-Dong Wang:** Writing — review & editing, Resources.

## **Conflict of interest statement**

The authors declare that they have no known competing financial interests or personal relationships that could have appeared to influence the work reported in this paper.

#### Acknowledgment

The authors would like to acknowledge the financial support provided by the National Key R&D Program of China (No. 2023YFB4104203 and No. 2022YFE0129900). The authors also wish to acknowledge the financial support from the National Natural Science Foundation of China (No. U22B2075). The funding from the Shandong Postdoctoral Science Foundation (No. SDBX2023017) is also greatly appreciated.

#### References

- Afanasyev, A., Vedeneeva, E., 2021. Compositional modeling of multicomponent gas injection into saline aquifers with the MUFITS simulator. J. Nat. Gas Sci. Eng. 94, 103988. https://doi.org/10.1016/j.jngse.2021.103988.
- Agada, S., Geiger, S., Elsheikh, A., et al., 2016. Data-driven surrogates for rapid simulation and optimization of WAG injection in fractured carbonate reservoirs. Pet. Geosci. 23 (2), 270–283. https://doi.org/10.1144/petgeo2016-068.
- Bocoum, A.O., Rasaei, M.R., 2023. Multi-objective optimization of WAG injection using machine learning and data-driven Proxy models. Appl. Energy 349, 121593. https://doi.org/10.1016/j.apenergy.2023.121593.
- Botechia, V.E., Correia, M.G., Rios, V., et al., 2023. Unisim-IV: benchmark proposal for light oil carbonate reservoir with high cO<sub>2</sub> content. Brazilian Journal of Petroleum and Gas 16 (4), 149–160. https://doi.org/10.5419/bjpg2022-0012.
- Cardoso, M.A., Durlofsky, L.J., 2010. Linearized reduced-order models for subsurface

- flow simulation. J. Comput. Phys. 229 (3), 681–700. https://doi.org/10.1016/j.jcp.2009.10.004.
- Chen, B., Reynolds, A.C., 2016. Ensemble-based optimization of the wateralternating-gas-injection process. SPE J. 21 (3), 786–798. https://doi.org/ 10.2118/173217-PA.
- CMG, 2023. CMG/GEM user guide/keywords/INVENTORY-CO<sub>2</sub>. Canada, Calgary: Computer Modeling Group 2023.
- Deb, K., Pratap, A., Agarwal, S., et al., 2002. A fast and elitist multiobjective genetic algorithm: NSGA-II. IEEE Trans. Evol. Comput. 6 (2), 182–197. https://doi.org/10.1109/4235.996017.
- Ding, S., Lu, R., Xi, Y., et al., 2020. Efficient well placement optimization coupling hybrid objective function with particle swarm optimization algorithm. Appl. Soft Comput. 95, 106511. https://doi.org/10.1016/j.asoc.2020.106511.
   Ding, S., Wen, F., Wang, N., et al., 2022. Multi-objective optimization of CO<sub>2</sub>
- Ding, S., Wen, F., Wang, N., et al., 2022. Multi-objective optimization of CO<sub>2</sub> enhanced oil recovery and storage processes in low permeability reservoirs. Int. J. Greenh. Gas Control 121, 103802. https://doi.org/10.1016/j.ijggc.2022.103802.
- Enab, K., Ertekin, T., 2021. Screening and optimization of CO<sub>2</sub>-WAG injection and fish-bone well structures in low permeability reservoirs using artificial neural network. J. Petrol. Sci. Eng. 200, 108268. https://doi.org/10.1016/ j.petrol.2020.108268.
- Fonseca, R.R.M., Chen, B., Jansen, J.D., et al., 2016. A stochastic simplex approximate gradient (StoSAG) for optimization under uncertainty. Int. J. Numer. Methods Eng. 109 (13), 1756–1776. https://doi.org/10.1002/nme.5342.
- Guerreiro, A.P., Fonseca, C.M., Paquete, L., 2021. The hypervolume indicator. ACM Comput. Surv. 54 (6), 1–42. https://doi.org/10.1145/3453474.
- He, J., Durlofsky, L.J., 2014. Reduced-order modeling for compositional simulation by use of trajectory piecewise linearization. SPE J. 19 (5), 858–872. https:// doi.org/10.2118/163634-PA.
- He, L., Zhao, F., He, W., 2024. Fingering inhibition triggered by CO<sub>2</sub> dissolution and viscosity reduction in water-alternating-CO<sub>2</sub> injection. Int. J. Heat Fluid Flow 110, 109646. https://doi.org/10.1016/j.ijheatfluidflow.2024.109646.
- Jansen, J.D., Fonseca, R.M., Kahrobaei, S., et al., 2014. The egg model—a geological ensemble for reservoir simulation. Geoscience Data Journal 1 (2), 192–195. https://doi.org/10.1002/gdj3.21.
- Klemetsdal, Ø.S., Møyner, O., Lie, K.A., 2019. Accelerating multiscale simulation of complex geomodels by use of dynamically adapted basis functions. Comput. Geosci. 24 (2), 459–476. https://doi.org/10.1007/s10596-019-9827-z.
- Leng, J., Bump, A., Hosseini, S.A., et al., 2024. A comprehensive review of efficient capacity estimation for large-scale CO<sub>2</sub> geological storage. Gas Science and Engineering 126, 205339. https://doi.org/10.1016/j.jgsce.2024.205339.
- Lie, K.A., Kedia, K., Skaflestad, B., et al., 2017. A general non-uniform coarsening and upscaling framework for reduced-order modeling. In: SPE Reservoir Simulation Conference. https://doi.org/10.2118/182681-MS.
- Liu, S., Yuan, B., Zhang, W., 2024. A new gradient-accelerated two-stage multiobjective optimization method for CO<sub>2</sub>-alternating-water injection in an oil reservoir. SPE J. 29 (5), 2445–2462. https://doi.org/10.2118/218392-PA.
- Ma, Z., Leung, J.Y., 2020. Design of warm solvent injection processes for heterogeneous heavy oil reservoirs: a hybrid workflow of multi-objective optimization and proxy models. J. Petrol. Sci. Eng. 191, 107186. https://doi.org/10.1016/j.petrol.2020.107186.
- Mohagheghian, E., James, L.A., Haynes, R.D., 2018. Optimization of hydrocarbon water alternating gas in the Norne field: application of evolutionary algorithms. Fuel 223, 86–98. https://doi.org/10.1016/j.fuel.2018.01.138.
- Nait-Amar, M., Ghahfarokhi, A., Ng, C.S.W., et al., 2021. Optimization of WAG in real geological field using rigorous soft computing techniques and nature-inspired algorithms. J. Petrol. Sci. Eng. 206, 109038. https://doi.org/10.1016/j.petrol.2021.109038.
- Olalotiti-Lawal, F., Onishi, T., Datta-Gupta, A., et al., 2019. Model calibration and optimization of a post-combustion CO<sub>2</sub> WAG pilot in a mature oil field. Fuel 255, 115810. https://doi.org/10.1016/j.fuel.2019.115810.
- Park, H.Y., Datta-Gupta, A., 2013. Reservoir management using streamline-based flood efficiency maps and application to rate optimization. J. Petrol. Sci. Eng. 109, 312–326. https://doi.org/10.1016/j.petrol.2013.06.004.
- Salehian, M., Çınar, M., 2019. Reservoir characterization using dynamic capacitance—resistance model with application to shut-in and horizontal wells. J. Pet. Explor. Prod. Technol. 9 (4), 2811–2830. https://doi.org/10.1007/s13202-019-0655-4.
- Storn, R., Price, K., 1997. Differential evolution—A simple and efficient adaptive scheme for global optimization over continuous spaces. J. Global Optim. 11 (4), 341—359. https://doi.org/10.1023/a:1008202821328.
- Tian, L., Huang, W., Tang, C., et al., 2024. Optimization of CO<sub>2</sub> water-gas alternating injection-production parameters in low permeability reservoirs. In: ASME 2024 43rd International Conference on Ocean, Offshore and Arctic Engineering. https://doi.org/10.1115/omae2024-127862.
- Ushmaev, O.S., Babin, V.M., Glavnov, N.G., et al., 2018. Efficient brownfield optimization of a reservoir in west Siberia. Pet. Geosci. 25 (2), 207–218. https://doi.org/10.1144/petgeo2018-022.
- van Doren, J.F.M., Markovinović, R., Jansen, J.D., 2006. Reduced-order optimal control of water flooding using proper orthogonal decomposition. Comput. Geosci. 10 (1), 137–158. https://doi.org/10.1007/s10596-005-9014-2.
- Zhao, M., Zhang, K., Chen, G., et al., 2020. A surrogate-assisted multi-objective evolutionary algorithm with dimension-reduction for production optimization. J. Petrol. Sci. Eng. 192, 107192. https://doi.org/10.1016/j.petrol.2020.107192.